THE JOURNAL OF PHYSICAL CHEMISTRY LETTERS
A JOURNAL OF THE AMERICAN CHEMICAL SOCIETY

pubs.acs.org/JPCL Letter

Nonadiabatic Dynamics of the Molecular Tully Models with the Mixed-Reference Spin-Flip Time-Dependent Density Functional Theory

Published as part of The Journal of Physical Chemistry Letters special issue "Wei-Hai Fang Festschrift".

Haiyi Huang, Juanjuan Zhang, Deping Hu,* and Ya-Jun Liu*

Cite This: *J. Phys. Chem. Lett.* 2025, 16, 13038−13045 Read Online

ACCESS | Metrics & More | Article Recommendations | Supporting Information

ABSTRACT: In this study, we perform on-the-fly nonadiabatic molecular dynamics (NAMD) simulations for three molecular systems (ethylene, DMABN, and fulvene), which are suggested as molecular versions of the Tully models, with the trajectory surface hopping method based on the mixed-reference spin-flip time-dependent density functional theory (MRSF-TDDFT). We employ several density functionals (CAM-B3LYP, M06-2X, BH&HLYP, and DTCAM-VAEE) in the MRSF-TDDFT calculations and compare the results with those obtained with the SA-CASSCF and MS-CASPT2 methods. For the ethylene molecule, the dynamics results obtained with MRSF-TDDFT compare very well with those obtained with MS-CASPT2, and the results with different functionals are similar. For the DMABN and fulvene molecules, the dynamics results with different functionals show certain differences, while the DTCAM-VAEE functional performs best among all functionals compared to MS-CASPT2. Moreover, for all molecules, MRSF-TDDFT outperforms SA-CASSCF for all functionals used in this work. We further explain the discrepancies of the dynamics results with different electronic structure methods through reaction pathway analysis. Overall, we strongly recommend the use of MRSF-TDDFT, especially with the DTCAM-VAEE functionals, in the NAMD simulations for complex molecular systems in the future, considering its good balance between accuracy and computational cost.

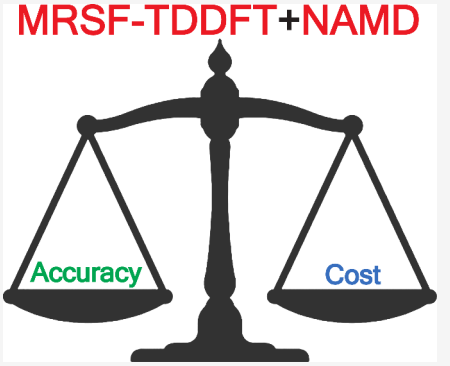

The nonadiabatic molecular dynamics (NAMD) simulations with the mixed quantum-classical (MQC) approaches are widely used to investigate photophysical and photochemical processes involving electronically nonadiabatic transitions.[1−3] The MQC methods treat nuclei classically and electrons quantum mechanically, as exemplified by the frequently used trajectory surface hopping (TSH) method.[4,5] We can naturally combine the TSH method with the on-the-fly dynamics, where the nuclei are evolving on a potential energy surface (PES) of one electronic state and can switch to another PES caused by the nonadiabatic effect. This underscores the critical importance of accurate PES descriptions in MQC dynamics.

For NAMD simulations of complex molecular systems, the PESs can be obtained from ab initio electronic structure calculations at each nuclear dynamics step. The most commonly used electronic structure calculation methods in NAMD include semiempirical methods,[6−11] complete active space self-consistent field (CASSCF),[12,13] multistate complete active space second-order perturbation theory (MS-CASPT2),[14,15] linear response time-dependent density functional theory (LR-TDDFT),[16,17] second-order approximate coupled-cluster singles and doubles (CC2),[18] and algebraic diagrammatic construction method to the second order [ADC(2)].[19,20] The semiempirical methods are dependent on parametrization and in most cases can only be applied reliably to molecules and elements that are included in their parametrization database.[21] The CASSCF method does not include the dynamics correction and tends to overestimate the excitation energies.[22] The MS-CASPT2 method includes the dynamic correlation through second-order perturbation theory and can achieve high accuracy, while it remains computationally feasible only for small systems.[23] The LR-TDDFT, CC2, and ADC(2) methods fail to correctly describe the conical intersections (CIs) between the ground state and excited states due to their single-reference nature.[24] The spin-flip variant of TDDFT (SF-TDDFT)[25,26] method has been developed to mitigate this defect, yet it suffers from spin contamination issues, limiting its applicability in NAMD simulations.

Received: October 14, 2025
Revised: November 26, 2025
Accepted: December 10, 2025
Published: December 12, 2025

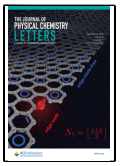

https://doi.org/10.1021/acs.jpclett.5c03195
J. Phys. Chem. Lett. 2025, 16, 13038−13045

Recently, the mixed-reference spin-flip TDDFT (MRSF-TDDFT) method has been put forward, which can overcome the inability of the conventional LR-TDDFT method to describe the multireference character of the electronic states, as well as the spin contamination issues inherent in SF-TDDFT.[27−42] Several studies have also applied MRSF-TDDFT in NAMD simulations and achieved great success in the investigation of various photophysical and photochemical processes.[41−48] Komarov et al. incorporated spin−orbit coupling into the MRSF-TDDFT framework and then investigated the intersystem crossing process in thymine via NAMD simulations.[41] After that, they introduced the doubly tuned exchange−correlation functionals to further improve the accuracy of MRSF-TDDFT and again assessed its performance on thymine through NAMD simulations.[42] Farmani et al. employed MRSF-TDDFT-based NAMD to elucidate the chemoexcitation dynamics underlying the conversion of firefly dioxetanone to oxyluciferin[43] and later investigated the competition between isomerization and ring-closure pathways in stilbene at various initial temperatures.[44] Sadiq and co-workers used MRSF-TDDFT combined with NAMD to examine the excited-state reactivity of prototropic cytosine tautomers.[45] Shostak et al. applied MRSF-TDDFT with NAMD simulations to reveal the ultrafast photochemical ring-opening mechanism of dihydroazulene.[46] Huix-Rotllant and collaborators combined MRSF-TDDFT with QM/MM-based NAMD to investigate the photochemistry of thymine in both solution and DNA environments.[47] Pomogaev et al. used MRSF-TDDFT with NAMD to study hydroxyl-bond predissociation in 4-methylphenol.[48]

However, a systematic study of the performance of MRSF-TDDFT in NAMD simulations is lacking. Hence, in this work, we aim to assess the performance of MRSF-TDDFT in NAMD across multiple molecular systems. To this end, we performed on-the-fly NAMD simulations using both MRSF-TDDFT (with various functionals) and CAS-based electronic structure methods (SA-CASSCF and MS-CASPT2) on three representative molecular systems: ethylene, DMABN, and fulvene. These systems serve as realistic analogues of Tully's models, exhibiting single avoided crossing, double avoided crossings, and reflection hopping events, respectively,[49] and have been widely used as molecular systems to test the performance of the NAMD methods.[50−58] We then analyzed and compared the results obtained using different electronic structure methods, culminating in an evaluation of the accuracy and applicability of MRSF-TDDFT in NAMD simulations.

To ensure consistency and comparability among the methods, all electronic quantities—including potential energies, energy gradients, and wave function overlaps—were computed using a range of theoretical approaches. Specifically, MRSF-TDDFT was applied with four typical exchange−correlation functionals: CAM-B3LYP,[59] M06-2X,[60] BH&HLYP,[61] and DTCAM-VAEE.[36] For benchmarking, multireference methods such as SA-CASSCF and MS-CASPT2 were also employed, with MS-CASPT2 serving as the reference method. The details of the electronic structure calculations and NAMD setups (trajectory convergence and decoherence correction tests) are presented in sections S1 and S2 in the Supporting Information. This work presents a comprehensive comparative analysis of NAMD results across these methods and systems, with a focus on both dynamic behavior and static properties, to evaluate the overall performance of MRSF-TDDFT in on-the-fly NAMD simulations.

For the ethylene molecular system, vertical excitation energies (VEEs) were calculated using MRSF-TDDFT, SA-CASSCF and MS-CASPT2 methods based on S_0 minimum optimized at the DFT level, the results are presented in Table 1. Compared to MS-CASPT2, SA-CASSCF significantly overestimates VEE, while MRSF-TDDFT with CAM-B3LYP functional underestimates it. Meanwhile, VEEs obtained using MRSF-TDDFT with M06-2X, BH&HLYP, and DTCAM-VAEE functionals are close to the VEE obtained from MS-CASPT2. For M06-2X and BH&HLYP functionals, the good performances in the description of the VEES are attributed to their high Hartree−Fock exchange composition compared to the CAM-B3LYP functional. The DTCAM-VAEE functional is designed for the MRSF-TDDFT calculations, and a detailed discussion about the advantages of this functional can be found in previous work.[31] The computed VEEs generally deviate from the experimental value, being either lower or higher by approximately 0.29−0.75 eV, whereas SA-CASSCF shows even larger error. In the following, we discuss the potential influence of such energetic errors on the excited-state lifetime and subsequent photoinduced dynamics.

Table 1. VEEs in eV for Ethylene Molecular System Obtained by MRSF-TDDFT with Different Functionals, SA-CASSCF and MS-CASPT2 Methods Based on the S_0 Minimum Optimized at BH&HLYP/def2-SVP Level

	transition pattern
method	$S_0 \rightarrow S_1$
CAM-B3LYP	7.37
M06-2X	8.22
BH&HLYP	8.18
DTCAM-VAEE	8.16
SA-CASSCF	10.13
MS-CASPT2	8.41
Exptl.[a]	7.66

[a]Ref 62.

The NAMD dynamics were initially determined at the S_1 state. During the dynamics simulations, the ethylene molecule undergoes an ultrafast nonadiabatic transition from the S_1 to the S_0 state via CIs. Two major types of S_0/S_1 CIs (pyramidalization and ethylidene) were located and optimized at the MS-CASPT2 level (Figure 1a) and were found to dominate among the CIs where the hopping events from S_1 to S_0 happen. Figure 1b presents the time-dependent population of the S_1 state by using different electronic structure calculation methods (further details of the evaluation of population are found in section S2 in Supporting Information). The population of the S_1 state shows an ultrafast decay within 200 fs for all of the electronic structure calculation methods. Notably, SA-CASSCF predicts the fastest population decay, while the population dynamics of the S_1 state are close to each other for MRSF-TDDFT and MS-CASPT2. The excited state lifetimes for different methods are also fitted and presented in Table S4. We can see that the calculated lifetimes are well consistent with the experimental lifetime for all methods.

To explain the dynamics results, we plotted the potential energy curves (PECs) from the FC region to pyramidalization and ethylidene CIs in Figure 1c,d, respectively. The PECs obtained by using MRSF-TDDFT with M06-2X, BH&HLYP,

https://doi.org/10.1021/acs.jpclett.5c03195
J. Phys. Chem. Lett. 2025, 16, 13038−13045

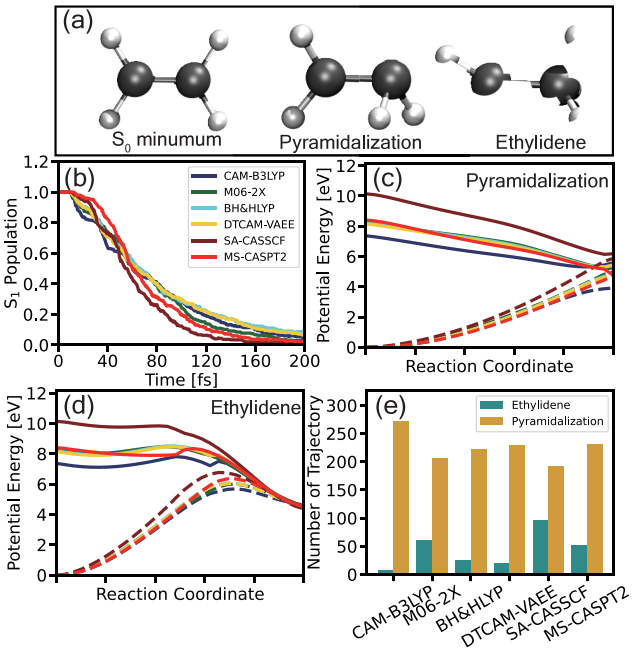

Figure 1. Results of the ethylene molecular system: (a) The S_0 minimum optimized at BH&HLYP/def2-SVP level and the S_0/S_1 CIs (pyramidalization and ethylidene types) optimized at MS-CASPT2-(2,2)/def2-SVP level. (b) Time-dependent population of the S_1 state during the dynamics. (c, d) PECs constructed though linear interpolation from the S_0 minimum to pyramidalization and ethylidene CIs. Solid and dashed lines correspond to the S_1 and S_0 states, respectively. (e) Distribution of the types of geometries where the $S_1 \rightarrow S_0$ hopping events happen for all trajectories with different electronic structural calculation methods.

and DTCAM-VAEE are in close agreement with those obtained using MS-CASPT2. However, PECs from SA-CASSCF and MRSF-TDDFT with CAM-B3LYP show certain deviations, with energies shifted upward and downward, respectively. For SA-CASSCF, the PEC shows a large steep slope from the FC region to pyramidalization CI. Meanwhile, the energy barrier from the FC region to ethylidene CI is very small. The above two factors lead to the fastest population decay of the S_1 state for SA-CASSCF in Figure 1b.

Figure 1e presents the distribution of the types of geometries where the $S_1 \rightarrow S_0$ hopping events occur for all trajectories. Since most of the hopping geometries can be classified into pyramidalization or ethylidene types, we counted only these two types of hopping geometries in this work. For all electronic structure calculation methods, the pyramidalization type dominates the hopping geometries, which can be explained by the PECs from the FC region to the pyramidalization CI being barrierless (see Figure 1c). Compared to MS-CASPT2, SA-CASSCF shows more frequent hopping via the ethylidene CI, due to the small energy barrier (0.08 eV) from the FC region to the ethylidene CI (Figure 1d). In contrast, for MRSF-TDDFT with the CAM-B3LYP functional, the number of ethylidene hopping geometries is very small, due to the large energy barrier (0.70 eV) from the FC region to the ethylidene CI (Figure 1d). For MRSF-TDDFT with M06-2X, BH&HLYP, and DTCAM-VAEE functionals, the ratios between the ethylidene and pyramidalization hopping geometries are close to that of MS-CASPT2, while the M06-2X functional performs the best among all functionals. This can also be explained by the energy barriers from the FC region to the ethylidene CI for M06-2X (0.45 eV), BH&HLYP (0.60 eV), and DTCAM-VAEE (0.57 eV) being close to that of MS-CASPT2 (0.45 eV) (Figure 1d).

Overall, the MRSF-TDDFT method, particularly when combined with M06-2X, BH&HLYP, and DTCAM-VAEE functionals, shows strong consistency with the MS-CASPT2 method in both static and dynamic descriptions of the ethylene system.

For the DMABN molecular system, we first computed the VEEs in the FC region using different electronic structure calculation methods, as summarized in Table 2. Like the

Table 2. VEEs with the Difference (ΔE) between Different Transition Patterns (in eV) for DMABN Molecular System Obtained by Using MRSF-TDDFT with Different Functionals, SA-CASSCF and MS-CASPT2 Based on the S_0 Minimum Optimized at BH&HLYP/def2-SVP Level

	transition pattern		
method	$S_0 \rightarrow S_1$	$S_0 \rightarrow S_2$	ΔE
CAM-B3LYP	4.39	5.11	0.72
M06-2X	4.57	5.29	0.72
BH&HLYP	4.61	5.36	0.75
DTCAM-VAEE	4.52	5.12	0.60
SA-CASSCF	4.79	6.64	1.85
MS-CASPT2	4.39	4.88	0.49
Exptl.[a]	4.13	4.57	0.44

[a]Ref 63.

ethylene system, the VEEs from S_0 to S_1 and S_2 obtained from MRSF-TDDFT with M06-2X, BH&HLYP, and DTCAM-VAEE functionals agree well with those from MS-CASPT2. Also like the ethylene system, MRSF-TDDFT with CAM-B3LYP functional underestimates the VEEs, while SA-CASSCF significantly overestimates the VEEs.

The population dynamics obtained from MS-CASPT2 (Figure 2a) shows an ultrafast decay from the S_2 to the S_1 state within 100 fs, with negligible population reaching the S_0 state. To explore the hopping mechanism, we analyzed several key internal coordinates (C1−C7, C7−N8, C1−C7−N8, C4−N13, ϕ, RMSD1, and RMSD2; see the definitions in the Supporting Information) for both the initial and hopping geometries (see Figures S8−S11 in the SI). We can see that the distributions of the key internal coordinates of the $S_2 \rightarrow S_1$ hopping geometries are similar to those of the initial geometries in the dynamics. The small geometry difference between the hopping geometries and the initial geometries is probably caused by the small S_1/S_2 energy gap in the FC region (0.49 eV obtained from MS-CASPT2; see Table 2). The results are also consistent with the early dynamics in the previous study,[64] where the shortening of the C1−C7 bond and elongation of the C7−N8 bond are also observed.

We could not successfully optimize the S_2/S_1 CI at the MS-CASPT2 level, either meeting a convergence problem or collapsing to irrelevant CIs (shown in Figure S7 in SI) which are not consistent with the hopping geometries for the DMABN molecule. We selected a representative $S_2 \rightarrow S_1$ hopping geometry, labeled as CI_{DMABN} (see the yellow circle in Figure S8f, Supporting Information), from the MS-CASPT2 trajectories for further analysis. The geometry of CI_{DMABN} and the corresponding geometry in the FC region are presented in Figure 2b. CI_{DMABN} with the shortening and elongation of C1−C7 and C7−N8 bonds from the FC region contributes the

https://doi.org/10.1021/acs.jpclett.5c03195
J. Phys. Chem. Lett. 2025, 16, 13038−13045

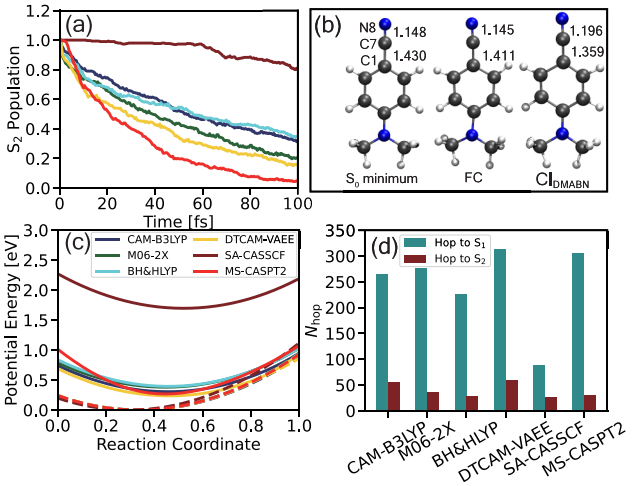

Figure 2. Results of the DMABN molecular system: (a) Time-dependent population of the S_2 state during the dynamics. (b) The S_0 minimum optimized at BH&HLYP/def2-SVP level and a geometry of the FC region and the corresponding representative hopping geometry (CI_{DMABN}) extracted from the NAMD at MS-CASPT2-(10,10)/def2-SV(P) level, with C1−C7 and C7−N8 bond lengths (Å) indicated. (c) PEC generated though linear interpolation from the FC region to CI_{DMABN}, respectively. Solid and dashed lines corresponds to the S_2 and S_1 states, respectively. (d) Hopping status (hopping counts from S_2 to S_1 and the contrary) of NAMD.

main hopping events. Figure 2c presents the PECs from the FC region to CI_{DMABN}, and Figure 2d shows the hopping events (double avoided crossings) during the NAMD.

We then carried out NAMD simulations by using MRSF-TDDFT with various functionals and the SA-CASSCF method. In the very early stage within 5 fs, MRSF-TDDFT predicts slightly faster population decay of the S_2 state than MS-CASPT2 (Figure 2a). Among all functionals, DTCAM-VAEE exhibits the best agreement with the MS-CASPT2 method, showing a similar overall decay profile. Other MRSF-TDDFT functionals (CAM-B3LYP, M06-2X, and BH&HLYP) produce similar dynamics among themselves, with slightly slower population decay. In addition, SA-CASSCF markedly underestimates the population decay rate.

To understand the dynamics differences, we examined the hopping geometries and PECs for the MRSF-TDDFT and SA-CASSCF methods. MRSF-TDDFT with all functionals and SA-CASSCF reproduces the same geometry change trends with shortened C1−C7 and elongated C7−N8 (see Figure S8 in the SI). The PECs from the FC region to CI_{DMABN} (Figure 2c) from MRSF-TDDFT are in close agreement with those from MS-CASPT2, whereas SA-CASSCF significantly overestimates the energy gap between S_1 and S_2 along the reaction pathway, resulting in its much slower population decay (Figure 2a). For MRSF-TDDFT dynamics, the S_2 state energies at the hopping geometry with respect to those at the initial geometries for MRSF-TDDFT are uniformly ∼0.4 eV higher than those for MS-CASPT2 dynamics (Figure S12, Supporting Information). This means that the system needs more potential energy to arrive at the hopping geometries, explaining the slightly slower population of the MRSF-TDDFT dynamics. Furthermore, the number of hoppings back to S_2 in MRSF-TDDFT with DTCAM-VAEE is larger than that in MS-CASPT2, as shown in Figure 2d. This leads to the faster population decay in MS-CASPT2 with a lower energy barrier along the reaction coordinate in spite of the larger energy gap between S_1 and S_2 (Table S5 in SI).

Overall, MRSF-TDDFT with CAM-B3LYP, M06-2X, BH&HLYP, and DTCAM-VAEE functionals yields similar PECs compared with the MS-CASPT2 method. For the population dynamics, the DTCAM-VAEE functional performs best among all the functionals. For SA-CASSCF, both the PEC and population dynamics are different from the MS-CASPT2 results.

For the fulvene molecular system, the VEEs calculated with different electronic structure methods are listed in Table 3.

Table 3. VEEs in eV for the Fulvene Molecular System Obtained by MRSF-TDDFT with Different Functionals, SA-CASSCF and MS-CASPT2 Based on the S_0 Minimum Optimized at BH&HLYP/def2-SVP Level

	transition pattern
method	$S_0 \rightarrow S_1$
CAM-B3LYP	3.55
M06-2X	3.50
BH&HLYP	3.64
DTCAM-VAEE	3.59
SA-CASSCF	4.24
MS-CASPT2	3.62
Exptl.[a]	3.34

[a]Ref 65.

The VEEs obtained by using MRSF-TDDFT with all functionals are close to that obtained by using MS-CASPT2, while SA-CASSCF largely overestimates the VEE. Meanwhile, the VEEs from both methods are both well consistent with the experimental value, with the exception of SA-CASSCF.

In the NAMD simulation, the system was initially placed in the S_1 state. To be consistent with the previous study,[49] the initial kinetic energy was set to zero. Here we will first elucidate the underlying dynamics mechanism based on the MS-CASPT2 results, followed by a comparison of performance across different electronic structure methods. After excitation to the S_1 state, the fulvene molecular system undergoes an ultrafast decay from the S_1 to the S_0 state. The time-dependent population of the S_1 state is shown in Figure 3a (solid yellow line), which exhibits two distinct decay regions separated by a plateau region. Specifically, decay regions occur at 10−15 fs and 28−34 fs, while plateau regions occur at 15−28 fs and 34−50 fs. The population is hard to fit, and we will not further discuss here the excited-state lifetime (approximated fitting lifetimes seen in Table S4 in SI).

To understand the mechanism, we optimized S_0/S_1 CI CI_{ful}, as shown in Figure 3b, under the constraint of freezing the torsion of the $-CH_2$ group. The C1−C6 bond length of CI_{ful} increases from 1.335 to 1.590 Å, consistent with the distribution of the C1−C6 bond lengths at the hopping geometries (Figure S13f in the SI). We also optimized the S_0/S_1 CI without constraint,; the geometry is shown in Figure S14 in the SI. This CI with the C1−C6 bond length of 1.472 Å and the C2−C1−C6−H8 dihedral angle of 112.1° differs from both the constrained CI_{ful} (Figure 3b) and the hopping geometries (Figure S13f in the SI). Therefore, the system primarily relaxes to the S_0 state through constrained CI CI_{ful}.

Figure S15f in the SI presents the distribution of the hopping events with time, including the $S_1 \rightarrow S_0$ and $S_0 \rightarrow S_1$ hopping. The two hopping regions correspond to the two

https://doi.org/10.1021/acs.jpclett.5c03195
J. Phys. Chem. Lett. 2025, 16, 13038−13045

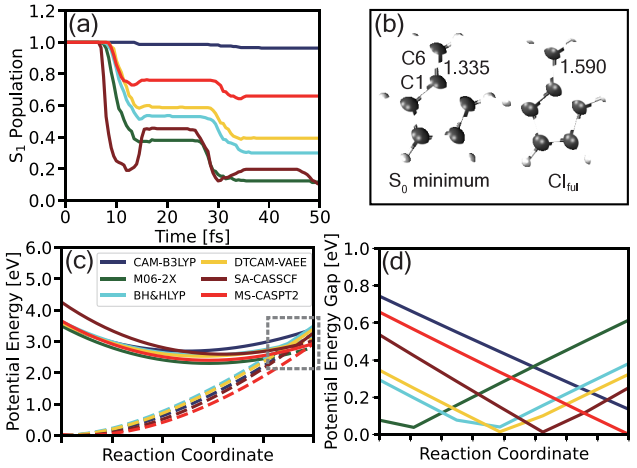

Figure 3. Results of the fulvene molecular system: (a) Time-dependent population of the S_1 state. (b) The S_0 minimum optimized at the BH&HLYP/def2-SVP level, while the S_0/S_1 CI optimized at the MS-CASPT2(6,6)/def2-SVP level, with the C1−C6 bond length indicated. (c) PECs generated through linear interpolation from the S_0 minimum to the CI_{ful}, where solid and dashed lines correspond to the S_1 and S_0 states, respectively. The gray dashed box highlights the enlarged region shown in panel d. (d) A detailed view of the region specified in panel c, illustrating the potential energy gap between the S_0 and S_1 states along the reaction coordinate.

decay regions in the population dynamics in Figure 3a, and no hopping is observed in the plateau region. Moreover, we found that the periodic population decay behavior of the S_1 state is relative to the vibrational motion of the C1−C6 bond (with a frequency of 1796.0 cm^{-1} and a period of ∼18.6 fs).

We further investigated the population dynamics resulting from other electronic structure calculation methods; the results are shown in Figure 3a. Within the first 15 fs, the populations of MRSF-TDDFT with BH&HLYP and DTCAM-VAEE functionals are very close to that of MS-CASPT2. After that, the populations also exhibit similar decay periods, although with faster decay rates. MRSF-TDDFT with M06-2X shows the fastest population decay of the S_1 state among the MRSF-TDDFT functionals, while CAM-B3LYP exhibits almost no population decay. Both of these results show large deviations from the MS-CASPT2 results. SA-CASSCF, by contrast, shows a rapid decay followed by substantial population return to the S_1 state, which is rarely seen in other methods (Figure S15 in the SI).

Figure 3c,d presents the PECs and the energy gap between the S_1 and S_0 states from the FC region to the CI_{ful}, respectively. The PECs of MRSF-TDDFT with M06-2X, BH&HLYP, and DTCAM-VAEE functionals are close to that of MS-CASPT2. The M06-2x predicts an earlier S_0/S_1 energy crossing point than MS-CASPT2, which may explain its faster population decay. CAM-B3LYP predicts a very late and high S_0/S_1 energy crossing point, which largely reduces the level of system hopping to the ground state. SA-CASSCF predicts the S_0/S_1 energy crossing point close to that of MS-CASPT2 but with a much steeper PECs decrease, resulting in the fastest transitions to the S_0 state. The large initial potential energy provides the system with sufficient kinetic energy to arrive at the CI_{ful} and then rebound, causing a pronounced population return to the S_1 state (Figure 3a). This behavior is distinct from other methods, which barely show population reverse from the S_0 to S_1 state.

Additionally, we performed the NAMD simulations with full initial kinetic energy (∼1.41 eV). The resulting population dynamics are shown in Figure S16 in the SI. Compared to the dynamics results above without initial kinetic energies, the S_1 lifetime is significantly shortened due to the enhanced access to the CI_{ful}. The decay periods remain synchronized with the C1−C6 vibrational mode, and the increased energy leads to a faster decay rate. The performances of the electronic structure methods are similar to those without initial kinetic energy, where MRSF-TDDFT with the DTCAM-VAEE functional performs best compared to the MS-CASPT2 results.

Overall, MRSF-TDDFT with BH&HLYP and DTCAM-VAEE functionals yields the closest population dynamics to that of MS-CASPT2, with DTCAM-VAEE providing the best agreement. M06-2X slightly overestimates the decay rate, while CAM-B3LYP significantly underestimates it. SA-CASSCF predicts the fastest population decay and exhibits pronounced reverse hopping events, highlighting its limitations for this system. To better show the performance of MRSF-TDDFT combined with NAMD, we carried out a simple computational cost test, shown in section S5 in the Supporting Information. In this test, the close accuracy, lower computational cost, and higher parallelization make MRSF-TDDFT a good alternative electronic calculation method to study NAMD.

In this study, we employ the MRSF-TDDFT method to investigate the nonadiabatic dynamics of three molecular Tully models: ethylene, DMABN, and fulvene. We perform the on-the-fly TSH dynamics by using the MRSF-TDDFT method with a range of functionals (CAM-B3LYP, M06-2X, BH&HLYP, and DTCAM-VAEE), as well as with the SA-CASSCF and MS-CASPT2 methods. For ethylene, whose PES along the reaction pathway shows a single crossing feature, the MRSF-TDDFT method produces population dynamics similar to the MS-CASPT2 method, while the SA-CASSCF method exhibits a slightly faster population decay. For DMABN, the MRSF-TDDFT method shows strong agreement with the MS-CASPT2 method, particularly when employing the DTCAM-VAEE functional, which yields the most accurate results among all the functionals. These findings underscore the reliability of the MRSF-TDDFT method in capturing dynamics involving more complex PESs. For fulvene, which is characterized by more intricate excited-state dynamics, the MRSF-TDDFT method with the DTCAM-VAEE and BH&HLYP functionals demonstrates the closest agreement with the MS-CASPT2 method, while notable discrepancies are observed when using the SA-CASSCF method and the MRSF-TDDFT method with other functionals. For all three molecular systems, the population dynamics and PESs computed using MRSF-TDDFT with DTCAM-VAEE functionals are largely consistent with the MS-CASPT2 results. In addition, the computational cost of the MS-CASPT2 method will largely increase with the size increase of the molecular system and the active space used, limiting the use of the MS-CASPT2 method in NAMD for relatively small molecular systems or with small active spaces. However, the MRSF-TDDFT method can be applied in NAMD for much larger molecular systems like the LR-TDDFT method. Considering its good performance in this work for the NAMD of the representative molecular system, we strongly recommend the use of MRSF-TDDFT, especially with the DTCAM-VAEE functional, in the study of the ultrafast nonadiabatic processes for larger and more complex systems in the future.

https://doi.org/10.1021/acs.jpclett.5c03195
J. Phys. Chem. Lett. 2025, 16, 13038−13045

■ ASSOCIATED CONTENT

Supporting Information

The Supporting Information is available free of charge at https://pubs.acs.org/doi/10.1021/acs.jpclett.5c03195.

Theoretical and computational details; additional analysis of trajectories; additional results for DMABN molecular system including the atom labels, distributions of key internal coordinates, the energy gaps and barriers between the FC region and CI_{DMABN}; additional results for fulvene molecular system, including the geometry of the optimized CI without constraint, distributions of key internal coordinates, time-dependent number of hop events, population dynamic with full initial kinetic energy; computational cost test; Cartesian coordinates for key geometries (PDF)

Transparent Peer Review report available (PDF)

■ AUTHOR INFORMATION

Corresponding Authors

Deping Hu − *Department of Chemistry, Faculty of Arts and Sciences, Center for Advanced Materials Research, Beijing Normal University, Zhuhai 519087, China;* orcid.org/0000-0001-7161-1253; Email: deping.hu@bnu.edu.cn

Ya-Jun Liu − *Department of Chemistry, Faculty of Arts and Sciences, Center for Advanced Materials Research, Beijing Normal University, Zhuhai 519087, China; Key Laboratory of Theoretical and Computational Photochemistry, Ministry of Education, College of Chemistry, Beijing Normal University, Beijing 100875, China;* orcid.org/0000-0001-8761-5339; Email: yajun.liu@bnu.edu.cn

Authors

Haiyi Huang − *Department of Chemistry, Faculty of Arts and Sciences, Center for Advanced Materials Research, Beijing Normal University, Zhuhai 519087, China*

Juanjuan Zhang − *SCNU Environmental Research Institute, Guangdong Provincial Key Laboratory of Chemical Pollution and Environmental Safety & MOE Key Laboratory of Environmental Theoretical Chemistry, School of Environment, South China Normal University, Guangzhou 510006, China;* orcid.org/0009-0003-3240-9257

Complete contact information is available at: https://pubs.acs.org/10.1021/acs.jpclett.5c03195

Notes

The authors declare no competing financial interest.

■ ACKNOWLEDGMENTS

This work was supported by grants from the Beijing Natural Science Foundation (Grant No. 2244074), the National Natural Science Foundation of China (Grant Nos. 22403008, 22373010, and 21973005), the Guangdong Basic and Applied Basic Research Foundation (Grant No. 2025A1515012183), and the start-up funding from Beijing Normal University (Grant No. 312200502511). Computing resources were provided by the Interdisciplinary Intelligence SuperComputer Center of Beijing Normal University at Zhuhai.

■ REFERENCES

(1) Domcke, W.; Koppel, H.; Yarkony, D. R. *Conical intersections: electronic structure, dynamics & spectroscopy*; World Scientific, 2004; Vol. *15*.

(2) Domcke, W.; Yarkony, D. *Conical intersections: theory, computation and experiment*; World Scientific, 2011; Vol. *17*.

(3) Crespo-Otero, R.; Barbatti, M. Recent Advances and Perspectives on Nonadiabatic Mixed Quantum−Classical Dynamics. *Chem. Rev.* **2018**, *118*, 7026−7068.

(4) Tully, J. C. Molecular dynamics with electronic transitions. *J. Chem. Phys.* **1990**, *93*, 1061−1071.

(5) Tully, J. C.; Preston, R. K. Trajectory Surface Hopping Approach to Nonadiabatic Molecular Collisions: The Reaction of H+ with D2. *J. Chem. Phys.* **1971**, *55*, 562−572.

(6) Granucci, G.; Toniolo, A. Molecular gradients for semiempirical CI wavefunctions with floating occupation molecular orbitals. *Chem. Phys. Lett.* **2000**, *325*, 79−85.

(7) Granucci, G.; Persico, M.; Toniolo, A. Direct semiclassical simulation of photochemical processes with semiempirical wave functions. *J. Chem. Phys.* **2001**, *114*, 10608−10615.

(8) Dewar, M. J. S.; Zoebisch, E. G.; Healy, E. F.; Stewart, J. J. P. Development and use of quantum mechanical molecular models. 76. AM1: a new general purpose quantum mechanical molecular model. *J. Am. Chem. Soc.* **1985**, *107*, 3902−3909.

(9) Stewart, J. J. P. Optimization of parameters for semiempirical methods II. Applications. *J. Comput. Chem.* **1989**, *10*, 221−264.

(10) Otte, N.; Scholten, M.; Thiel, W. Looking at Self-Consistent-Charge Density Functional Tight Binding from a Semiempirical Perspective. *J. Phys. Chem. A* **2007**, *111*, 5751−5755.

(11) Cusati, T.; Granucci, G.; Martínez-Núñez, E.; Martini, F.; Persico, M.; Vázquez, S. Semiempirical Hamiltonian for Simulation of Azobenzene Photochemistry. *J. Phys. Chem. A* **2012**, *116*, 98−110.

(12) Roos, B. O.; Taylor, P. R.; Sigbahn, P. E. A complete active space SCF method (CASSCF) using a density matrix formulated super-CI approach. *Chem. Phys.* **1980**, *48*, 157−173.

(13) Roos, B. O. Advances in Chemical Physics. *Advances in Chemical Physics* **1987**, *69*, 399−445.

(14) Andersson, K.; Malmqvist, P. A.; Roos, B. O.; Sadlej, A. J.; Wolinski, K. Second-order perturbation theory with a CASSCF reference function. *J. Phys. Chem.* **1990**, *94*, 5483−5488.

(15) Andersson, K.; Malmqvist, P.; Roos, B. O. Second-order perturbation theory with a complete active space self-consistent field reference function. *J. Chem. Phys.* **1992**, *96*, 1218−1226.

(16) Runge, E.; Gross, E. K. U. Density-Functional Theory for Time-Dependent Systems. *Phys. Rev. Lett.* **1984**, *52*, 997−1000.

(17) CASIDA, M. E. *Recent Advances in Density Functional Methods; Recent Advances in Computational Chemistry* Vol. 1; World Scientific, 1995; Vol. *1*; pp 155−192.

(18) Christiansen, O.; Koch, H.; Jørgensen, P. The second-order approximate coupled cluster singles and doubles model CC2. *Chem. Phys. Lett.* **1995**, *243*, 409−418.

(19) Trofimov, A B; Schirmer, J An efficient polarization propagator approach to valence electron excitation spectra. *Journal of Physics B: Atomic, Molecular and Optical Physics* **1995**, *28*, 2299.

(20) Dreuw, A.; Wormit, M. The algebraic diagrammatic construction scheme for the polarization propagator for the calculation of excited states. *WIREs Computational Molecular Science* **2015**, *5*, 82−95.

(21) Silva-Junior, M. R.; Thiel, W. Benchmark of Electronically Excited States for Semiempirical Methods: MNDO, AM1, PM3, OM1, OM2, OM3, INDO/S, and INDO/S2. *J. Chem. Theory Comput.* **2010**, *6*, 1546−1564.

(22) Helmich-Paris, B. Benchmarks for Electronically Excited States with CASSCF Methods. *J. Chem. Theory Comput.* **2019**, *15*, 4170−4179.

(23) Sarkar, R.; Loos, P.-F.; Boggio-Pasqua, M.; Jacquemin, D. Assessing the Performances of CASPT2 and NEVPT2 for Vertical Excitation Energies. *J. Chem. Theory Comput.* **2022**, *18*, 2418−2436.

(24) Matsika, S. Electronic Structure Methods for the Description of Nonadiabatic Effects and Conical Intersections. *Chem. Rev.* **2021**, *121*, 9407−9449.
(25) Rinkevicius, Z.; Vahtras, O.; Agren, H. Spin-flip time dependent density functional theory applied to excited states with single, double, or mixed electron excitation character. *JOURNAL OF CHEMICAL PHYSICS* **2010**, *133*, 114104.
(26) Bernard, Y. A.; Shao, Y.; Krylov, A. I. General formulation of spin-flip time-dependent density functional theory using non-collinear kernels: Theory, implementation, and benchmarks. *JOURNAL OF CHEMICAL PHYSICS* **2012**, *136*, 204103.
(27) Lee, S.; Filatov, M.; Lee, S.; Choi, C. H. Eliminating spin-contamination of spin-flip time dependent density functional theory within linear response formalism by the use of zeroth-order mixed-reference (MR) reduced density matrix. *J. Chem. Phys.* **2018**, *149*, 104101.
(28) Lee, S.; Kim, E. E.; Nakata, H.; Lee, S.; Choi, C. H. Efficient implementations of analytic energy gradient for mixed-reference spin-flip time-dependent density functional theory (MRSF-TDDFT). *JOURNAL OF CHEMICAL PHYSICS* **2019**, *150*, 184111.
(29) Lee, S.; Park, W.; Choi, C. H. Expanding Horizons in Quantum Chemical Studies: The Versatile Power of MRSF-TDDFT. *ACCOUNTS OF CHEMICAL RESEARCH* **2025**, *58*, 208−217.
(30) Mironov, V.; Komarov, K.; Li, J.; Gerasimov, I.; Nakata, H.; Mazaherifar, M.; Ishimura, K.; Park, W.; Lashkaripour, A.; Oh, M.; Huix-Rotllant, M.; Lee, S.; Choi, C. H. OpenQP: A Quantum Chemical Platform Featuring MRSF-TDDFT with an Emphasis on Open-Source Ecosystem. *JOURNAL OF CHEMICAL THEORY AND COMPUTATION* **2024**, *20*, 9464−9477.
(31) Park, W.; Lee, S.; Komarov, K.; Mironov, V.; Nakata, H.; Zeng, T.; Huix-Rotllant, M.; Choi, C. H. MRSF-TDDFT: A new tool in quantum chemistry for better understanding molecules and materials. *BULLETIN OF THE KOREAN CHEMICAL SOCIETY* **2025**, *46*, 330−346.
(32) Komarov, K.; Mironov, V.; Lee, S.; Pham, B. Q.; Gordon, M. S.; Choi, C. H. High-performance strategies for the recent MRSF-TDDFT in GAMESS. *JOURNAL OF CHEMICAL PHYSICS* **2023**, *158*, 194105.
(33) Horbatenko, Y.; Lee, S.; Filatov, M.; Choi, C. H. Performance Analysis and Optimization of Mixed-Reference Spin-Flip Time-Dependent Density Functional Theory (MRSF-TDDFT) for Vertical Excitation Energies and Singlet-Triplet Energy Gaps. *JOURNAL OF PHYSICAL CHEMISTRY A* **2019**, *123*, 7991−8000.
(34) Lashkaripour, A.; Park, W.; Mazaherifar, M.; Choi, C. H. Addressing the High-Throughput Screening Challenges of Inverted Singlet-Triplet Materials by MRSF-TDDFT. *JOURNAL OF CHEMICAL THEORY AND COMPUTATION* **2025**, *21*, 5661−5668.
(35) Horbatenko, Y.; Sadiq, S.; Lee, S.; Filatov, M.; Choi, C. H. Mixed-Reference Spin-Flip Time-Dependent Density Functional Theory (MRSF-TDDFT) as a Simple yet Accurate Method for Diradicals and Diradicaloids. *JOURNAL OF CHEMICAL THEORY AND COMPUTATION* **2021**, *17*, 848−859.
(36) Park, W.; Lashkaripour, A.; Komarov, K.; Lee, S.; Huix-Rotllant, M.; Choi, C. H. Toward Consistent Predictions of Core/Valence Ionization Potentials and Valence Excitation Energies by MRSF-TDDFT. *JOURNAL OF CHEMICAL THEORY AND COMPUTATION* **2024**, *20*, 5679.
(37) Baek, Y. S.; Lee, S.; Filatov, M.; Choi, C. H. Optimization of Three State Conical Intersections by Adaptive Penalty Function Algorithm in Connection with the Mixed-Reference Spin-Flip Time-Dependent Density Functional Theory Method (MRSF-TDDFT). *JOURNAL OF PHYSICAL CHEMISTRY A* **2021**, *125*, 1994−2006.
(38) Park, W.; Komarov, K.; Lee, S.; Choi, C. H. Mixed-Reference Spin-Flip Time-Dependent Density Functional Theory: Multireference Advantages with the Practicality of Linear Response Theory. *JOURNAL OF PHYSICAL CHEMISTRY LETTERS* **2023**, *14*, 8896−8908.
(39) Park, W.; Alias-Rodriguez, M.; Cho, D.; Lee, S.; Huix-Rotllant, M.; Choi, C. H. Mixed-Reference Spin-Flip Time-Dependent Density Functional Theory for Accurate X-ray Absorption Spectroscopy. *JOURNAL OF CHEMICAL THEORY AND COMPUTATION* **2022**, *18*, 6240.
(40) Komarov, K.; Oh, M.; Nakata, H.; Lee, S.; Choi, C. H. UMRSF-TDDFT: Unrestricted Mixed-Reference Spin-Flip-TDDFT. *JOURNAL OF PHYSICAL CHEMISTRY A* **2024**, *128*, 9526−9537.
(41) Komarov, K.; Park, W.; Lee, S.; Zeng, T.; Choi, C. H. Accurate Spin-Orbit Coupling by Relativistic Mixed-Reference Spin-Flip-TDDFT. *JOURNAL OF CHEMICAL THEORY AND COMPUTATION* **2023**, *19*, 953.
(42) Komarov, K.; Park, W.; Lee, S.; Huix-Rotllant, M.; Choi, C. H. Doubly Tuned Exchange-Correlation Functionals for Mixed-Reference Spin-Flip Time-Dependent Density Functional Theory. *JOURNAL OF CHEMICAL THEORY AND COMPUTATION* **2023**, *19*, 7671−7684.
(43) Farmani, M.; Lee, S.; Zeng, T.; Choi, C. H. Chemoexcited Formation and Radiationless Decay Dynamics of Firefly Chromophore. *JOURNAL OF PHYSICAL CHEMISTRY LETTERS* **2024**, *15*, 9518−9524.
(44) Farmani, M.; Park, W.; Lee, S.; Choi, C. H. Tipping the ultrafast photochemical balance of cis-stilbene. *PHOTOCHEMICAL & PHOTOBIOLOGICAL SCIENCES* **2025**, *24*, 955−962.
(45) Sadiq, S.; Park, W.; Mironov, V.; Lee, S.; Filatov Gulak, M.; Choi, C. H. Prototropically Controlled Dynamics of Cytosine Photodecay. *JOURNAL OF PHYSICAL CHEMISTRY LETTERS* **2023**, *14*, 791−797.
(46) Shostak, S.; Park, W.; Oh, J.; Kim, J.; Lee, S.; Nam, H.; Filatov, M.; Kim, D.; Choi, C. H. Ultrafast Excited State Aromatization in Dihydroazulene. *JOURNAL OF THE AMERICAN CHEMICAL SOCIETY* **2023**, *145*, 1638−1648.
(47) Huix-Rotllant, M.; Schwinn, K.; Pomogaev, V.; Farmani, M.; Ferre, N.; Lee, S.; Choi, C. H. Photochemistry of Thymine in Solution and DNA Revealed by an Electrostatic Embedding QM/MM Combined with Mixed-Reference Spin-Flip TDDFT. *JOURNAL OF CHEMICAL THEORY AND COMPUTATION* **2023**, *19*, 147−156.
(48) Pomogaev, V.; Bocharnikova, E.; Avramov, P.; Tchaikovskaya, O. p-cresol quantum-classical photodynamics, photostatic UV, IR and Raman spectra. *JOURNAL OF MOLECULAR STRUCTURE* **2025**, *1344*, 142986.
(49) Ibele, L. M.; Curchod, B. F. E. A molecular perspective on Tully models for nonadiabatic dynamics. *Phys. Chem. Chem. Phys.* **2020**, *22*, 15183−15196.
(50) Weight, B. M.; Mandal, A.; Huo, P. Ab initio symmetric quasi-classical approach to investigate molecular Tully models. *J. Chem. Phys.* **2021**, *155*, 084106.
(51) Weight, B. M.; Mandal, A.; Hu, D.; Huo, P. Ab initio spin-mapping non-adiabatic dynamics simulations of photochemistry. *J. Chem. Phys.* **2025**, *162*, 084105.
(52) Mannouch, J. R.; Kelly, A. Quantum Quality with Classical Cost: Ab Initio Nonadiabatic Dynamics Simulations Using the Mapping Approach to Surface Hopping. *J. Phys. Chem. Lett.* **2024**, *15*, 5814−5823.
(53) Toldo, J. M.; Mattos, R. S.; Pinheiro, M. J.; Mukherjee, S.; Barbatti, M. Recommendations for Velocity Adjustment in Surface Hopping. *J. Chem. Theory Comput.* **2024**, *20*, 614−624.
(54) T do Casal, M.; Toldo, J. M.; Pinheiro, M. J.; Barbatti, M. Fewest switches surface hopping with Baeck-An couplings. *Open research Europe* **2021**, *1*, 49−49.
(55) Ibele, L. M.; Memhood, A.; Levine, B. G.; Avagliano, D. Ab Initio Multiple Spawning Nonadiabatic Dynamics with Different CASPT2 Flavors: A Fully Open-Source PySpawn/OpenMolcas Interface. *J. Chem. Theory Comput.* **2024**, *20*, 8140−8151.
(56) Gómez, S.; Spinlove, E.; Worth, G. Benchmarking non-adiabatic quantum dynamics using the molecular Tully models. *Phys. Chem. Chem. Phys.* **2024**, *26*, 1829−1844.
(57) Richardson, J. O.; Lawrence, J. E.; Mannouch, J. R. Nonadiabatic Dynamics with the Mapping Approach to Surface Hopping (MASH). *Annu. Rev. Phys. Chem.* **2025**, *76*, 663−687.

https://doi.org/10.1021/acs.jpclett.5c03195
J. Phys. Chem. Lett. 2025, 16, 13038−13045

(58) Souza Mattos, R.; Mukherjee, S.; Barbatti, M. Legion: A Platform for Gaussian Wavepacket Nonadiabatic Dynamics. *J. Chem. Theory Comput.* **2025**, *21*, 2189−2205.
(59) Yanai, T.; Tew, D. P.; Handy, N. C. A new hybrid exchange−correlation functional using the Coulomb-attenuating method (CAM-B3LYP). *Chem. Phys. Lett.* **2004**, *393*, 51−57.
(60) Zhao, Y.; Truhlar, D. G. The M06 suite of density functionals for main group thermochemistry, thermochemical kinetics, noncovalent interactions, excited states, and transition elements: two new functionals and systematic testing of four M06-class functionals and 12 other functionals. *Theor. Chem. Acc.* **2008**, *120*, 215−241.
(61) Becke, A. D. A new mixing of Hartree−Fock and local density-functional theories. *J. Chem. Phys.* **1993**, *98*, 1372−1377.
(62) Leang, S. S.; Zahariev, F.; Gordon, M. S. Benchmarking the performance of time-dependent density functional methods. *J. Chem. Phys.* **2012**, *136*, 104101.
(63) Druzhinin, S. I.; Mayer, P.; Stalke, D.; von Bülow, R.; Noltemeyer, M.; Zachariasse, K. A. Intramolecular Charge Transfer with 1-tert-Butyl-6-cyano-1,2,3,4-tetrahydroquinoline (NTC6) and Other Aminobenzonitriles. A Comparison of Experimental Vapor Phase Spectra and Crystal Structures with Calculations. *J. Am. Chem. Soc.* **2010**, *132*, 7730−7744.
(64) Kochman, M. A.; Tajti, A.; Morrison, C. A.; Miller, R. J. D. Early Events in the Nonadiabatic Relaxation Dynamics of 4-(N,N-Dimethylamino)benzonitrile. *J. Chem. Theory Comput.* **2015**, *11*, 1118−1128.
(65) Asmis, K. R.; Allan, M.; Schafer, O.; Fülscher, M. Electron-Energy-Loss Spectroscopy and Theoretical Study of Triplet and Singlet Excited States of Fulvene. *J. Phys. Chem. A* **1997**, *101*, 2089−2095.

https://doi.org/10.1021/acs.jpclett.5c03195
J. Phys. Chem. Lett. 2025, 16, 13038−13045